water

MDPI

Article

A Multidisciplinary Approach for Clarifying the Recharge Processes and Origin of Saline Water in the Semi-Arid Punata Alluvial fan in Bolivia

Andres Gonzales Amaya [1,2,*], Gerhard Barmen [2] and Galo Muñoz [2]

[1] Teknisk Geologi, Lund University, Lund 22100, Sweden
[2] Laboratório de Hidráulica, Universidad Mayor de San Simón, 1832 Cochabamba, Bolivia; gerhard.barmen@tg.lth.se (G.B.); galomunoz.v@fcyt.umss.edu.bo (G.M.)
* Correspondence: andres.gonzales@tg.lth.se; Tel.: +46-222-74-25

Received: 28 June 2018; Accepted: 11 July 2018; Published: 16 July 2018

Abstract: The analysis of stable isotopes assisted in identifying that groundwater in the Punata alluvial fan is mainly recharged by heavy flash floods, and the recharge from rainfall is of less importance. In addition, the hydrochemical analysis identified the Pucara River as the main source of recharge. Other streams in the north and northwest of the fan do not seem to contribute to the recharge. The hydrochemistry also shows that there is an increase of the Na^+ and Cl^- concentrations in the middle and distal part of the fan. The salinization of groundwater is most likely a result of the mixing of fresh water with residual saline pore water in the lacustrine deposits and/or ion exchange within these layers. Geophysical surveys assisted in describing the aquifer system layering, and indicated a fine-grained bottom layer where ion exchange might occur. This study demonstrates that the integration of several methods (e.g., hydrochemistry, hydrogeophysics, and stable isotopes) is valuable for clarifying ambiguities during the interpretation process and for characterizing hydrogeological processes in alluvial fans in general.

Keywords: stable isotopes; hydrochemistry; geophysics; groundwater recharge; salinization

1. Introduction

Surface water access is considered to play a crucial role for the development of economic and social activities, but groundwater reserves can be as important as surface water and can thus play a similar role especially in arid and semiarid regions of the world [1–3]. Alluvial fans are generally located in arid and semi-arid zones, and they have the nature of having permeable layers where water can be stored, thus, they can be important sources of water supply. For sustainable management of groundwater, however, knowledge of origin, recharge process, flow direction, and mineralization is needed.

Different approaches for understanding groundwater processes across the world have been presented in the literature, e.g., Burbery and Vincent [4]; Edmunds and Droubi [5]; Fetter [6], Han, et al. [7]; Hassen, Hamzaoui-Azaza, and Bouhlila [1]; Herczeg, et al. [8]; Stimson, et al. [9]; Yuan, et al. [10]; and, Zhang, Song, Zhang, Han, Tang, Yu, and Ma [3]. For instance, Kolsi, et al. [11] used multivariate statistical approach and stable isotope analysis obtaining valuable information about hydrogeological parameters. Herczeg, Dogramaci, and Leaney [8] used a combination of stable isotope and hydrochemical analysis to evaluate the origin of dissolved salts and solutes in groundwater in the Murray basin, Australia. These approaches proved that the integration of different techniques could help in identifying sources of solutes, such as salinization.

In Bolivia, there is generally a lack of comprehensive research which can provide knowledge of importance for the planning of further sustainable strategies for groundwater exploitation. The Punata

alluvial fan is an overexploited area, which is located in the department of Cochabamba, see Figure 1a. In this semiarid area, the river surface water is scarce and the precipitation rates are low, which leads to a deficit in water supply. This deficit has caused a rise in borehole drilling and groundwater exploitation. For a sustainable water management in the Punata area, it is thus important to identify the recharge sources of the groundwater and the groundwater flow paths. To date, however, there are contradictory reports in the literature. Some local reports state that the Pucara River is the main recharge source, i.e., United Nations Developing Program (UNDP) and Geological Bureau of Bolivia (GEOBOL) report: UNDP-GEOBOL [12]; while others, i.e., Hernandez [13] and Alvarado, et al. [14], claim that, besides the Pucara River, local streams and cracks in bedrock are equally important in the recharge process. Moreover, local reports indicate that groundwater quality in some boreholes is not apt for human consumption and irrigation purposes due to the high content of salts. The main objective of this study is to clarify these ambiguities regarding the Punata alluvial fan. Another aim is to show the benefits of combining different approaches, such as stable isotopes, hydrochemistry, and hydrogeophysics for providing information about the recharge process, flow patterns, and causes for groundwater salinization in semiarid alluvial fans.

2. Methodology

2.1. Study Area

The Punata alluvial fan is located in the central part of Bolivia (Figure 1a), in the department of Cochabamba between the coordinates latitude 17.59° S–17.49° S and longitude 65.90° W–65.7° W. The study area is surrounded by a mountainous massif, which peaks can reach 4600 m above sea level (m.a.s.l.), and gently slopes from the northeast to the southwest. The extent of the alluvial fan is around 90 km^2, and the main urban center is the Punata city in the middle of the fan. The hydrological Pucara basin (Figure 1a), which is the northeast upper neighbor catchment, drains the runoff of this basin through the Pucara River. Also, lakes in the highlands of the Pucara basin discharge water to the Pucara River. The discharge zone of the Pucara River is in the apex of the Punata fan. Besides Pucara River, there are small streams in the eastern and northern part of the fan, i.e., Pocoata River and San Benito and Paracaya streams.

The annual potential evapotranspiration can be greater than 950 mm, while the average annual precipitation is around 350 mm, thus reflecting the semiarid conditions of the study area. The rainy season normally takes place between November and April, and about 80% of the annual precipitation falls between December and February. During the dry season, the flow of local creeks and rivers is minimum, and they barely reach the Punata fan. The local aquifer system is generally unconfined close to the apex of the fan, and it is semiconfined to confined towards the middle and distal part of the fan. The depth of the water table ranges between 10 and 15 m below ground surface in the distal part of the fan, to 35 and 40 m in the head of the fan. Yields from boreholes range from less than 0.5 L/s in the distal part of the fan to 18 L/s in the head of the fan.

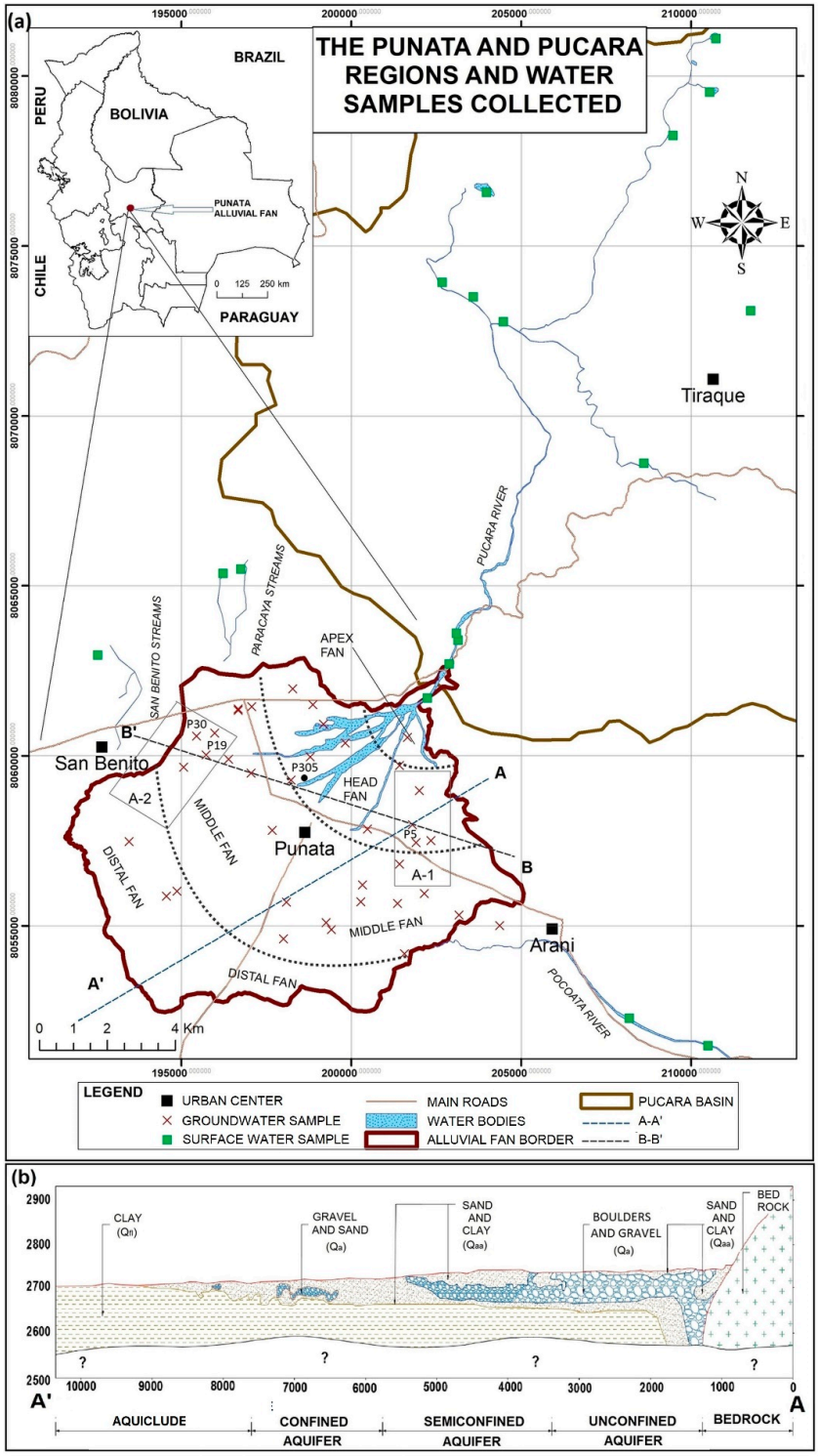

Figure 1. (**a**) Study area and location of water samples. The water samples are classified in surface water and groundwater; (**b**) Cross section of the Punata alluvial fan, where the question mark means that the depth to bedrock is still unknown, from Gonzales Amaya, et al. [15].

The regional geology is described by UNDP-GEOBOL [12], GEOBOL [16], and May, et al. [17]. The basement of the study area is formed of Ordovician rocks. These rocks are mainly limonite and quartz sandstone. Overlying Silurian formations consist of alternating strata of micaceous minerals and reddish and blackish shales. Dolostone, marlstone and limestone are the typical rocks in the Cretaceous

formations, which overlie the Silurian deposits. The valleys are filled with unconsolidated sediments from the Quaternary, the main units are: fluvial, lacustrine, fluviolacustrine, and colluvial-alluvial sediments. These units form terraces on riverbanks and also beds and alluvial fans at the mouths of creeks and rivers. During the lower Pliocene, due to the uplift of the mountain massif, tectonic valleys and closed lakes were created. The climate in this period was predominately dry and saline material with high clay content was deposited [12]. Figure 1b shows the deposition of Quaternary sediments in the Punata alluvial fan, as follows: (1) In the apex of the fan, fluvial (Qa) and terrace sediments were deposited. These deposits are mainly composed of coarse material, varying from boulders to sand; (2) The middle of the fan is a transitory zone from alluvial (Qaa) to fluvio-lacustrine (Qfl) deposits. The grain size of these deposits ranges from gravel to silt and clay; (3) The distal part of the fan is mainly composed of fluvio-lacustrine deposits (Qfl) and the deposits are finegrained and mainly composed of silt and clay.

2.2. Water and Soil Sample Collection

This study included a total of 57 samples from two different sources: groundwater and surface water (Tables 1 and 2). The samples from groundwater are located within the Punata fan, while the latter are distributed along surface water bodies in the neighboring basins. The sampling depth of groundwater depended on the position of the well screens, which are often located at the bottom of the borehole. However, there are some wells that have screens at different depths. Table 2 provides information about the depth of sampling in wells and the aquifer unit where the bottom screen is located. The samples were spatially distributed in order to take into consideration all the possible recharge sources. At each sampling location, Electrical Conductivity (EC) and pH values were measured. The water samples were analyzed at the Center of Water and Environmental Sanitation (Centro de Aguas y Saneamiento Ambiental) within the Universidad Mayor de San Simon (UMSS) in Bolivia. The analyses include total dissolved solids (TDS), major ions such as calcium (Ca^{2+}), magnesium (Mg^{2+}), sodium (Na^{+}) bicarbonate ($HCO_3{}^{-}$), chloride (Cl^{-}), sulfate ($SO_4{}^{2-}$); and, minor species, such as potassium (K^{+}), and nitrate ($NO_3{}^{-}$). The concentrations are given in milligram per liter (mg/L), while EC is presented in micro Siemens per centimeter (µS/cm). The water sampling followed the protocol and standards methods of APHA [18]. After purging the boreholes, the water samples were collected in 500 mL sterilized polyethylene bottles and stored below 4 °C until the analysis was performed. Bicarbonate was determined by H_2SO_4 titration (with a mixed indicator bromocresol green-methyl red, and corroborated with an end-point pH measurement). Sulfate and chlorides were determined with the turbidimetric and argentometric methods, respectively. While the rest of ions were determined by ionic chromatography. For the stable isotope analyses (^{2}H and ^{18}O), a total of 45 water samples were collected. The saturation indexes (SI) for Halite were estimated by using PHREEQC [19] software assuming a mean air pressure and solution temperature of 1 atm and 25 °C, respectively. The stable isotope analyses were carried out at the laboratory of the Geological Survey of Denmark and Greenland. The analyses were carried out using a Cavity Ring-Down Spectroscopy (CRDS) method and a PICARRO L2120 Isotopic Water Analyzer (precision of <0.2‰ and <0.6‰ for ^{18}O and ^{2}H, respectively). The samples were collected in 50 and 25 mL sterilized polyethylene bottles with watertight caps and stored below 4 °C. The isotopic compositions are reported as the deviation (δ) of the ratio of the heavy isotopes (^{18}O and ^{2}H) to the light ones (^{16}O and ^{1}H) of a sample from that of the VSMOW (Vienna Standard Mean Ocean Water) in parts per thousand, ‰.

A total of 20 top soil samples were collected within the Punata fan (Figure 2). The samples are mainly located in the head of the fan due to the fact that in this area it is expected to have a greater variation in the soil physical properties when compared to the middle and distal parts of the fan where the top soil is mostly clayey. In each location, soil samples were collected and infiltration tests were performed, both at three different depths: 30, 50 and 100 cm below the surface. The following physical properties were determined in the laboratory: texture, bulk density (ϱ), field capacity (θ_{fc}), wilting point (θ_{wp}), total porosity (n), and content of gravel, sand, clay, and silt. The infiltration surveys

were performed with a Guelph permeameter, and when conditions were not suitable (i.e., coarse soil) the double ring infiltrometer was used. The estimation of the hydraulic conductivity (*K*) was done by applying the approaches that are defined in Reynolds and Elrick [20] and Elrick, et al. [21]. In order to verify the consistence of the estimates, these were compared with the values from the ROSETTA software [22]. ROSETTA uses a neural network analysis to estimate hydraulic parameter, such as *K*. This software can use limited information (i.e., grain size distribution) or more detailed information (i.e., grain size distribution, bulk density, porosity, wilting point, and/or field capacity) for the estimation of *K*.

2.3. Ion Chemistry and Chemical Weathering Process

Multiple techniques were used to visualize and analyze the hydrochemical processes occurring within the study area. Scatter plots and Chadha diagrams [23] were used to help in the task of distinguishing patterns and relationships in the aquifer system. Many studies, e.g., Han, et al. [24], Edmunds, et al. [25], and Herczeg, et al. [26], demonstrated that the concentration of major ions is a function of the direction and distance of groundwater flow. Weathering processes are important when interpreting the ion concentrations in the water sample. By performing chemical analysis of groundwater samples, it is possible to track the mineral weathering occurred along a groundwater path within an aquifer system. Appelo and Postma [27], Marion [28], Drever [29], and Datta and Tyagi [30] summarize some of the typical known weathering reactions, and how these reactions are associated to the weathering of some minerals and rocks (e.g., halite dissolution).

The ability of ion exchange is an important phenomenon and determines the mobility of some chemical elements. Ion exchange sites are often found in clay and organic soil materials, and some authors have proposed the following ordering of cation exchangeability [6,27]: $Na^+ > K^+ > Mg^{2+} > Ca^{2+}$, the divalent ions tend to replace the monovalent ions, but it is reversible and at high activities the monovalent ions can replace the divalent ions. The relation of $[(Ca^{2+} + Mg^{2+})\text{-}(HCO_3^- + SO_4^{2-})]$ and $(Na^-\text{-}Cl^-)$ were used by several authors (e.g., Bouzourra, et al. [31], García, et al. [32], and Jalali [33]), for determining the gain or loss of $(Ca^{2+} + Mg^{2+})$ due to silicate weathering and/or ion exchange, while $(Na^+\text{-}Cl^-)$ shows the gain or the loss of Na^+ provided by evaporates.

2.4. Stable Isotopes

The application of stable isotope analysis can provide a better understanding of some hydrogeological processes. The environmental isotopes, such as oxygen-18 (^{18}O) and deuterium (^{2}H), are non-anthropogenic and natural. They can assist in the understanding of hydrochemical problems, for instance, in the identification of recharge sources and flow patterns, and also in the development of a water budget [34]. The occurrence of ^{18}O and ^{2}H in groundwater might have a meteoric origin, therefore there is a strong bond between these isotope concentrations and the values of precipitation reflected in the Global Meteoric Water Line (GMWL); this relationship is given by a slope of 8 and a ^{2}H excess of +10‰ [35]. Deviations from the GMWL can be interpreted as being caused by local or regional climatic condition, or by precipitation that occurred during warmer or colder climate than at present. The main effects that cause deviations from the GMWL are temperature, amount effect, evaporation, and altitude [36].

3. Results

3.1. Stable Isotopes Composition

The stable isotopic ratio of the water samples ranged from −14.5‰ to −9.6‰ for $\delta^{18}O$ and from −106.5‰ to −77.9‰ for $\delta^{2}H$ (refer to Table 1). Rainfall records from the researches [9,37–39] are used for comparison, since it was not possible to collect rainfall samples within the study area. Stimson, Frape, Drimmie, and Rudolph [9] collected five rainfall water samples in the northwestern

nearby basin of Cochabamba. The Cochabamba basin is located 40 km away, and has similar climate and physiographic characteristics. The rainfall samples from Cochabamba were collected during the months of January to June, and have been used for defining a local meteoric water line (LMWL): $\delta^2H = 7.8\delta^{18}O + 11$. In the study area the groundwater samples showed less variation in the isotopic composition than samples from surface water, and have similar values than the ones that are found in [37]. Both surface water and groundwater samples are shifted to the right of the GMWL (refer to Figure 3) highlighting the evaporation processes within the samples. A local evaporation water line (LWEL) was estimated: $\delta^2H = 5.6\delta^{18}O - 24$.

Table 1. $\delta^{18}O$ and δ^2H both in ‰ versus Vienna Standard Mean Ocean Water (VSMOW). The letters G, R, and S in the field Type stands for groundwater, rainfall, and surface water, respectively. R type samples are for comparison from Stimson, Frape, Drimmie and Rudolph [9].

ID	Type	Sampling Date	$\delta^{18}O$	δ^2H	ID	Type	Sampling Date	$\delta^{18}O$	δ^2H
P1	G	Nov-15	−11.9	−93.2	P26	G	Jul-16	−13.4	−100.5
P2	G	Nov-15	−13.1	−98.9	P27	G	Jul-16	−13.2	−99.2
P3	G	Nov-15	−12.4	−94.7	P28	G	Jul-16	−13.4	−101.3
P4	G	Nov-15	−13.7	−101.4	P29	G	Jul-16	−13.0	−99.3
P5	G	Nov-15	−13.5	−101.2	P30	G	Jul-16	−12.7	−96.9
P6	G	Nov-15	−12.6	−96.4	P31	S	Jul-16	−11.2	−85.2
P7	G	Nov-15	−12.2	−96.7	P32	S	Aug-16	−13.2	−96.2
P9	S	Oct-15	−9.6	−80.1	P33	S	Aug-16	−12.6	−91.9
P10	S	Oct-15	−9.8	−79.0	P35	S	Aug-16	−11.5	−90.8
P11	G	Nov-15	−12.9	−98.7	P36	S	Aug-16	−10.5	−85.2
P12	G	Dec-15	−13.1	−100.1	P37	S	Aug-16	−9.7	−77.9
P13	G	Dec-15	−14.1	−106.4	P38	S	Aug-16	−12.9	−94.9
P14	G	Dec-15	−13.5	−104.0	P39	S	Aug-16	−12.6	−97.1
P15	G	Dec-15	−13.3	−100.1	P40	G	Aug-16	−13.1	−98.1
P16	G	Dec-15	−12.7	−96.9	P41	G	Aug-16	−12.9	−98.7
P17	G	Dec-15	−13.1	−99.4	P42	G	Aug-16	−12.8	−97.4
P18	G	Dec-15	−12.3	−97.0	P43	S	Aug-16	−14.5	−105.3
P19	G	Dec-15	−12.9	−98.0	P44	S	Aug-16	−14.3	−104.3
P20	G	Dec-15	−13.0	−98.2	P45	S	Aug-16	−13.5	−98.9
P21	G	Dec-15	−13.2	−99.1	P58	R	Jan-90	−8.4	−58.8
P22	G	Jul-16	−13.2	−99.0	P59	R	Jan-90	−10.1	−59.1
P23	G	Jul-16	−13.0	−97.3	P60	R	Mar-90	−12.1	−79.8
P24	G	Jul-16	−12.7	−95.8	P61	R	Mar-90	−11.5	−75.9
P25	G	Jul-16	−13.3	−100.1	P62	R	Jul-90	−10.1	−78.4

3.2. General Ions Trends

The physicochemical results of the 57 water samples are listed in Table 2. It can be noted that there are some variations among the collected samples, especially for EC, Na^+, Cl^- and TDS. This is most likely due to the fact that groundwater samples in the distal part of the fan (e.g., northwestern part) have longer flow paths, and have dissolved more minerals, which increase the TDS, and consequently, the EC.

The concentration of the major elements ranges widely, for instance, concentrations of Cl^- and Na^+ can range from 0.12 to 1515 mg/L and from 2.2 to 1370 mg/L, respectively. HCO_3^-, Ca^{2+}, Cl^-, Na^+ and SO_4^{2-} are the ions with the higher concentrations, while concentrations of NO_3^- showed the lowest values. Statistical analysis showed that TDS, EC, Na^+, Cl^-, HCO_3^- and Ca_2^+ are the most important parameters for describing the water samples. From these parameters, the dominant ions (i.e., Ca^{2+}, HCO_3^-, Cl^- and Na^+) can be related to origin of solutes in water from natural processes of mineral (rock) dissolution, ion exchange, or transport of solutes.

Table 2. Physicochemical components of groundwater and surface water in the study area. All the units are in mg/L, with exception of EC in μS/cm, pH dimensionless, and depth in meters. In the column aquifer U, SC, and SW stands for unconfined, semiconfined, and surface water.

ID	Depth	Aquifer	pH	EC	Ca^{2+}	Mg^{2+}	K^{+}	Na^{+}	HCO_3^{-}	Cl^{-}	SO_4^{2-}	NO_3^{-}	TDS	SI Halite
P1	120	U	7.3	181	16	5	2	12	74	4	13	1.2	128	−8.8
P2	80	SC	7.6	1619	32	2	3	253	173	350	56	1.2	871	−5.6
P3	85	U	7.9	191	20	3	2	12	81	5	13	1.2	137	−8.8
P4	65	U	7.7	190	6	2	3	29	80	7	12	0.9	140	−8.2
P5	70	U	7.6	367	14	2	3	47	93	45	18	1.5	224	−7.2
P6	100	U	7.6	345	16	4	2	64	85	47	16	1.4	234	−7.1
P7	95	U	7.7	446	11	3	3	94	95	74	12	0.8	293	−6.7
P8	0	SW	7.5	213	19	5	7	14	93	5	4	<0.1	147	−8.7
P9	0	SW	8.4	192	20	3	3	13	90	5	10	0.2	144	−8.7
P10	0	SW	9	191	19	4	3	13	89	4	11	0.1	144	−8.8
P11	65	U	7.6	198	15	4	2	22	99	7	12	1	163	−8.4
P12	60	SC	8	635	12	2	3	91	157	89	1	0.6	357	−6.6
P13	60	SC	8.4	599	6	2	3	93	158	77	29	0.1	369	−6.7
P14	100	SC	8.4	806	16	2	3	145	226	110	23	0.6	526	−6.4
P15	65	U	7.6	184	12	4	2	20	78	8	12	0.9	137	−8.3
P16	90	U	7.5	164	11	4	1	18	70	5	12	0.7	122	−8.6
P17	70	U	7.8	190	16	5	3	16	78	5	16	1.2	140	−8.7
P18	70	SC	7.5	348	19	5	2	36	84	51	14	0.5	213	−7.3
P19	70	SC	7.7	508	22	13	3	49	100	87	18	0.6	292	−6.9
P20	75	SC	8	529	24	6	2	51	101	87	23	0.5	296	−6.9
P21	75	U	7.1	452	21	6	2	50	106	68	19	1.2	290	−7.0
P22	110	SC	7.2	1555	44	10	3	267	207	314	58	0.9	922	−5.7
P23	90	SC	7.6	942	12	6	2	235	196	159	35	0.8	666	−6.0
P24	100	U	7.4	157	9	4	1	21	83	4	12	0.5	156	−8.6
P25	85	U	7.2	186	13	4	2	21	84	11	12	0.9	164	−8.2
P26	85	U	7.4	551	14	7	2	85	140	86	17	1.3	373	−6.7
P27	60	SC	7.3	179	15	7	2	19	90	5	36	1.4	199	−8.6
P28	70	SC	7.6	1945	40	7	3	418	229	437	7	0.9	1161	−5.3
P29	70	SC	6.9	570	30	10	2	63	106	100	40	1.3	377	−6.8
P30	50	SC	8.6	2407	24	12	5	527	199	604	12	0.3	1408	−5.1
P31	0	SW	8.0	70	8	2	1	2	31	0	8	1.3	59	−11.1
P32	0	SW	8.2	114	7	8	1	12	46	<0.1	25	0.1	108	−10.4
P33	0	SW	7.7	92	12	8	1	3	56	<0.1	2	0.3	95	−10.9
P34	0	SW	8.0	116	6	7	5	6	56	4	2	0.2	88	−9.2
P35	0	SW	9.1	228	8	12	3	45	116	6	18	<0.1	268	−8.1
P36	0	SW	8.0	273	8	12	5	37	139	16	7	<0.1	240	−7.8
P37	0	SW	9.3	240	20	8	3	29	132	5	21	<0.1	227	−8.4
P38	0	SW	7.3	42	3	1	1	5	27	<0.1	1	<0.1	46	−10.7
P39	0	SW	7.7	232	11	6	2	50	127	6	3	0.6	215	−8.1
P40	60	SC	6.9	323	14	6	2	36	88	43	19	1.3	224	−7.4
P41	95	U	6.8	168	14	6	1	19	84	4	16	1	160	−8.6
P42	100	U	6.9	281	18	3	1	35	99	29	19	0.8	217	−7.5
P43	0	SW	6.7	34	1	1	1	6	20	<0.1	2	1.1	41	−10.6
P44	0	SW	6.8	39	3	1	1	7	31	<0.1	2	0.9	52	−10.6
P45	0	SW	7.3	69	5	2	1	12	52	1	2	1.5	84	−9.8
P46	128	SC	7.5	5765	110	34	3	1370	286	1515	336	0.8	3670	−4.4
P47	82	SC	7.3	856	17	6	2	189	82	205	73	9.9	600	−6.0
P48	85	U	6.9	375	15	6	1	71	83	54	20	0.8	270	−7.0
P49	70	U	6.8	144	7	3	2	23	65	3	6	0.2	154	−8.7
P50	85	SC	7.2	598	25	14	2	82	174	64	28	0.2	411	−6.8
P51	17	SC	7.5	393	22	6	1	157	109	38	35	0.1	370	−6.8
P52	50	SC	7.4	1087	64	17	1	165	214	139	121	<0.1	744	−6.2
P53	60	SC	7.6	294	6	3	1	157	75	43	7	<0.1	293	−6.7
P54	0	SW	7.0	81	7	2	2	6	22	3	2	1.2	48	−9.2
P55	0	SW	6.8	95	6	4	8	9	32	7	<0.1	1	72	−8.7
P56	0	SW	6.9	61	6	2	2	4	20	3	11	1.4	37	−9.5
P57	90	SC	7.4	293	10	3	0	54	77	42	10	2.7	198	−7.2

3.3. Top Soil Samples

Table 3 summarizes the laboratory results that were obtained from the top soil samples. The grain size distribution of the soil samples decreases in size from the apex towards the distal part of the fan. In the same way, the values of *K* tend to be greater within the head of the fan and smaller in the distal and mid of the fan. Figure 2a shows the texture classification of the soil samples, where three different points clusters can be distinguished. The first of them have higher percentages of sand and all of these samples are located within the apex and the head of the fan. While the other two clusters have higher

percentages of silt and clay, and they are located mainly within the middle and distal part of the fan. The difference in percentages might be explained due to the fact that energy of Pucara River is greater close to the apex, therefore carries coarser material. While towards the middle and distal part of the fan the energy of the river decreases, and therefore transports only finer material such as clay and silt.

Table 3. Location and physical properties of the top soil samples collected in the Punata alluvial fan.

ID	UTM Coordinates		Fan Region	Content (%)			ϱ (g/cm^3)	θ_{fc} (%)	θ_{wp} (%)	n (%)	K (cm/d)
	X	Y		Gravel and Sand	Silt	Clay					
K1	198810	8059131	Mid fan	68.0	7.0	25.0	1.7	14.9	7.2	35.6	95.8
K2	199730	8060065	Fan head	28.0	32.0	40.0	1.4	21.8	10.2	47.9	26.8
K3	201056	8061288	Fan head	90.0	1.0	9.0	1.5	15.3	7.8	42.9	43.1
K4	201004	8060021	Fan head	59.0	14.0	27.0	1.5	15.5	7.7	42.6	45.1
K5	200929	8059093	Fan head	80.0	6.0	14.0	1.8	11.9	5.9	34.2	206.3
K6	200915	8058216	Fan head	41.0	21.0	38.0	1.4	15.8	6.4	47.5	25.1
K7	200792	8056997	Mid fan	82.0	3.0	15.0	2.0	10.6	5.2	26.0	112.4
K8	202227	8060657	Fan head	23.0	35.0	42.0	1.6	19.5	9.8	42.0	22.5
K9	202188	8060029	Fan head	83.0	2.0	15.0	1.7	12.7	6.3	38.1	101.3
K10	197485	8061473	Mid fan	80.0	40.0	30.0	1.3	25.1	14.3	50.6	30.4
K11	195396	8062381	Mid fan	82.0	2.0	16.0	1.5	11.9	5.4	42.4	154.4
K12	204216	8055790	Mid fan	30.0	54.0	16.0	1.3	29.3	18.6	51.2	70.8
K13	192275	8059483	Distal fan	26.0	50.0	24.0	1.3	24.3	13.4	48.8	29.0
K14	195373	8056029	Distal fan	34.0	44.0	22.0	1.3	29.5	18.6	51.1	30.4
K15	195340	8053997	Distal fan	18.0	33.0	49.0	1.6	17.4	8.6	41.6	30.2
K16	196457	8052727	Distal fan	30.0	41.0	29.0	1.4	26.1	13.7	48.0	14.9
K17	198608	8056960	Mid fan	23.0	59.0	18.0	1.3	23.7	13.3	52.8	44.1
K18	198642	8054014	Distal fan	38.0	40.0	22.0	1.4	24.4	9.5	46.7	19.9
K19	200784	8055889	Mid fan	36.0	54.0	10.0	1.5	30.3	17.4	44.3	28.5
K20	202957	8054360	Distal fan	24.0	36.0	40.0	1.4	23.2	11.6	47.9	26.5

Figure 2b displays the values and distribution of K at three different depths (i.e., 30, 50 and 100 cm). In general, the values of K are smaller at depths of 30 cm, and greater at depths of 50 and 100 cm. Also, it is possible to suggest that K values are greater in the apex and head of the fan, than the ones on the distal and middle parts of the fan. The difference between K values are mainly due to the fact that coarser material is more likely in the apex and head of the fan, which increases the values of K.

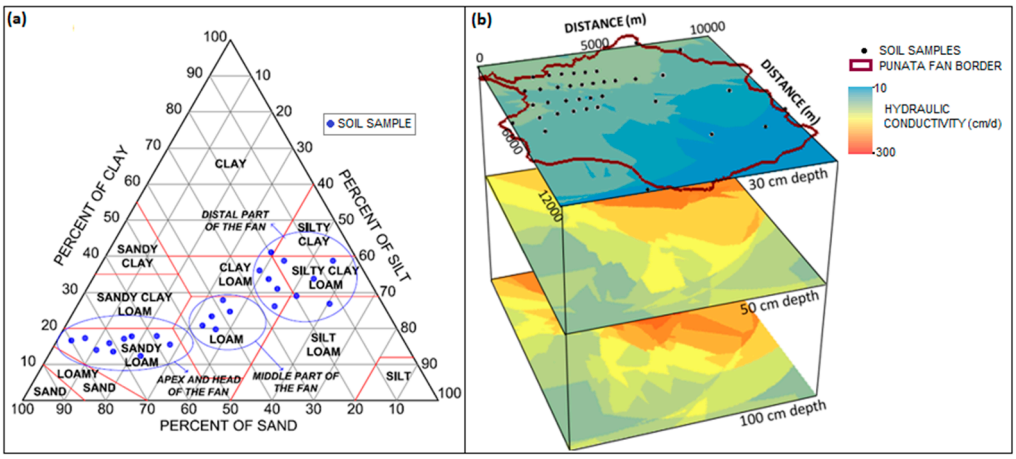

Figure 2. (**a**) Classification of soil texture by percentage of clay, sand and silt; (**b**) Spatial variation of hydraulic conductivity at depths of 30, 50 and 100 cm.

4. Discussion

4.1. Groundwater Recharge

The composition of stable isotopes in the Punata alluvial fan is similar to those generally found in semi-arid and arid regions, which are dominated by evaporation signatures, e.g., The rainfall that takes place in the study area come from the Amazon basin (i.e., origin in the Atlantic ocean), therefore the depleted values in rainfall samples (i.e., −12.1‰ to −8.4‰ for $\delta^{18}O$ and −79.8‰ to −58.8‰ for $\delta^{2}H$), as found by [9], for the neighboring Cochabamba basin are expected since the study area is a region further inland from the Atlantic ocean. The LMWL of the study area (Figure 3) is similar to the one found by [40] in the northern region of Chile ($\delta^{2}H = 7.7\delta^{18}O + 9.7$), and the one found in [39] as obtained from samples in a transect from the Bolivian Amazon to the Andes range ($\delta^{2}H = 8.0\delta^{18}O + 15.2$). The slope of these studies are lower or equal than eight from the GMWL, which probably is explained by an amount effect: during heavy rainfalls the isotopic composition tends to decrease with time due to a continuous isotopic exchange within the raindrops and the air mass below the storm [41]. Groundwater and surface water samples in the study areas have an evaporation trend, which is similar to the one found in Oruro [42], at 150 km west from the Punata region. The LEWL from Oruro has a slope of 5, and since both Punata and Oruro areas receive storms primarily from the Amazon basin, and Punata is somewhat more humid than Oruro, the LEWL in Punata (Figure 3) should have a slope slightly higher than 5 (i.e., 5.6). The LMWL slopes from Punata and Oruro fit with the description that in arid and semi−arid regions the evaporation trends have slopes as low as 4 to 6, highlighting the recycling of evaporated water into cloud masses [43].

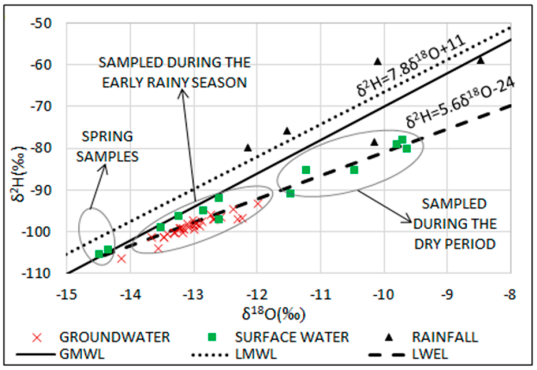

Figure 3. Isotopic (^{2}H and ^{18}O) variations in groundwater, rainfall, and surface water samples. The global meteoric water line (GMWL), the local meteoric water lines (LMWL), and the local evaporation water line (LEWL) are also displayed.

The surface waters in Figure 3 are clustered in three groups, which probably are due the fact that samples were collected in different seasons. Samples collected during the dry period would tend to be more isotopically enriched due to evaporation effects, while samples that were collected during the rainy period might tend to be more depleted probably due to the amount effect explained above. Two surface water samples were clearly more depleted than the rest of the samples; the locations of these samples are springs that are located in the neighbor basin (Paracaya streams, refer to Figure 1a). These springs may be the discharge areas of water infiltrated within the secondary porosity of the surrounding Ordovician rocks, hence the isotopic composition cannot be explained by evaporation because they are located within the GMWL highlighting a meteoric origin. Therefore, one explanation might be that these waters have been infiltrated during different climate conditions where meteoric waters were more isotopically depleted. However, more investigation is needed in this area to fully understand the local hydrological processes.

Groundwater samples showed less variation regarding isotopic composition, with an approximately variation of 2‰ and 13‰ for $\delta^{18}O$ and $\delta^{2}H$, respectively. Groundwater samples have similar isotopic composition with samples of surface water collected during the rainy season. The rainy season in the study area is characterized by heavy storms of short duration, which usually originates flash flood events. Since the heavy storms may be more isotopically depleted, the originated flash floods would be depleted as well, which is in line with the similar isotopic composition with groundwater samples and surface water samples that were collected during rainy season. On the other hand, some groundwater samples located within the middle and distal part of the fan are more isotopically enriched, which might be due to vertical infiltration of evaporated water. However, this pattern is not reproduced entirely in all of the samples located in the distal and middle part of the fan, suggesting that the infiltration from the local streams during heavy floods is the predominant recharge process within the aquifer system. Hence, it might be suggested that light rainfalls, which are more enriched in $\delta^{18}O$ and $\delta^{2}H$, are of minor importance in the recharge process. Consequently, heavy storms, which lead to heavy flash floods events, are of major importance for the recharge process in the Punata alluvial fan.

4.2. Origin of Saline Water

The water chemistry in the study area generally evolves from Ca^{2+}/Na^{+}-HCO_3^- to Na^{+}-Cl^- water type. Figure 4a shows that surface water have predominately higher concentrations of HCO_3^-, the arrows in this figure resemble the flow directions: water from rivers and streams infiltrates into the aquifer system and flows towards the distal part of the fan. Surface water from Pucara and Pocoata River have similar composition (i.e., Ca^{2+}-HCO_3^- type), while Paracaya and San Benito surface waters have lower ion concentration and are more Na+ enriched (e.g., Na^{+}-HCO_3^- water type). In the distal part of the fan, the water type is dominated by higher concentrations of Na^{+} and Cl^-. Four possible hypothesis might explain the increased salinization of the groundwater: (1) dissolution of halite; (2) infiltration of irrigation waters and/or excess on the use of fertilizers; (3) vertical diffuse recharge through the unsaturated soil; (4) or due to the existence of saline deposits lying in the lacustrine bottom of the local aquifer system.

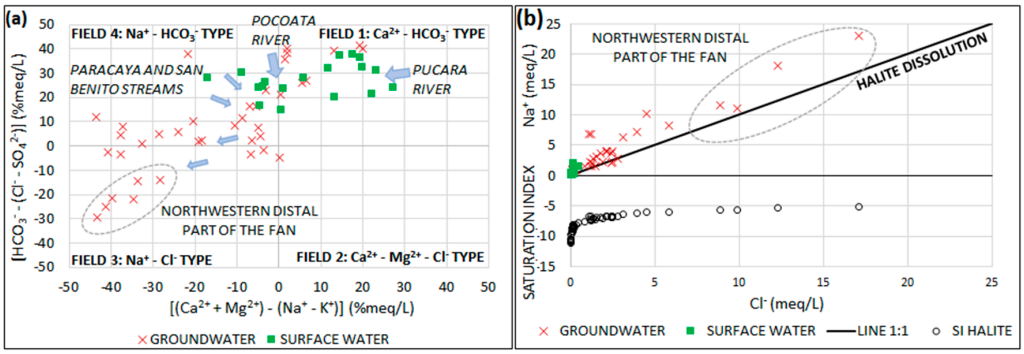

Figure 4. (**a**) Chadha diagram showing the groundwater classification, concentrations of ions are expressed as a percentage of total meq/L. The arrows resemble the flow direction and the evolution of the chemical composition of water samples; (**b**) Bivariate plot of Cl^- versus Na^{+}, and saturation indexes of halite versus Cl^-.

When hypothesis (1) was analyzed it would have been expected that the dissolution of halite in water released equal concentration of Na^{+} and Cl^-, but the results from this study deviates slightly from the expected 1:1 relation (Figure 4b). Most of the points are above the 1:1 line, which means that the concentration of Na^{+} is higher than Cl^-. Figure 4b also displays the saturation indexes (SI) with respect to halite, which are, on average, at least a factor of 8 less than the saturation point. Moreover,

the local geology does not describe any halite deposit close to the study area. These indicators conduct to reject the hypothesis (1) that the dissolution of halite is the source of groundwater salinization.

For hypothesis (2) and (3); first, a spatial analysis of the ion concentrations in the study areas was done in order to identify the possible recharge areas and chemical evolution of groundwater samples. Figure 5 shows the circular diagrams with the concentration of the major ions in water samples. The samples that were located in the northernmost part of the Punata fan are not displayed because surface water in overall has a similar chemical composition. Groundwater samples that were located in the discharge areas of Pucara and Pocoata Rivers have similar chemical composition as the surface samples; hence, this strengthens the isotopic analyses that suggest that the Punata groundwater is mainly recharged by river flows. Groundwater samples tend to increase the TDS towards the distal part of the fan. However, the northwestern border of the fan yielded the highest TDS, where Na^+ and Cl^- are the dominant ions. If vertical infiltration would have been even in all of the study area, and since the crops and irrigation practices are, in general, the same in the Punata fan, it would be expected to find groundwater samples with more or less the same ion concentrations. Moreover, the most used method for irrigation in the agricultural lands of the study area is by flooding the terrains. Due to the semiarid conditions of the region, it would be expected that part of the irrigation water would be evaporated and/or transpired by plants, therefore salt ions would be deposited in the soil. After heavy rainfalls or when irrigation water is not evaporated nor transpired, it would be expected that water would infiltrate downwards, and hence, transporting all the solutes. However, the groundwater samples yielded very low concentrations with respect to NO_3^- (refer to Table 2), which indicates that there is no contamination from human activities, such as septic pits or fertilizers, even though such activities take place within the Punata fan. Therefore, the low concentration values of NO_3^- suggests that reduction processes occurred during infiltration, or that the water infiltrating vertically does not reach the sampled groundwater. Since the genesis of an alluvial fan entails an interfingering of different deposits with different grain sizes, it is probable that lenses with high concentration of clay in the unsaturated zone might act as a semipermeable barrier that prevents the vertical infiltration to reach the groundwater. Hence, it seems that hypothesis (2) and (3) do not explain the groundwater salinization in the study area.

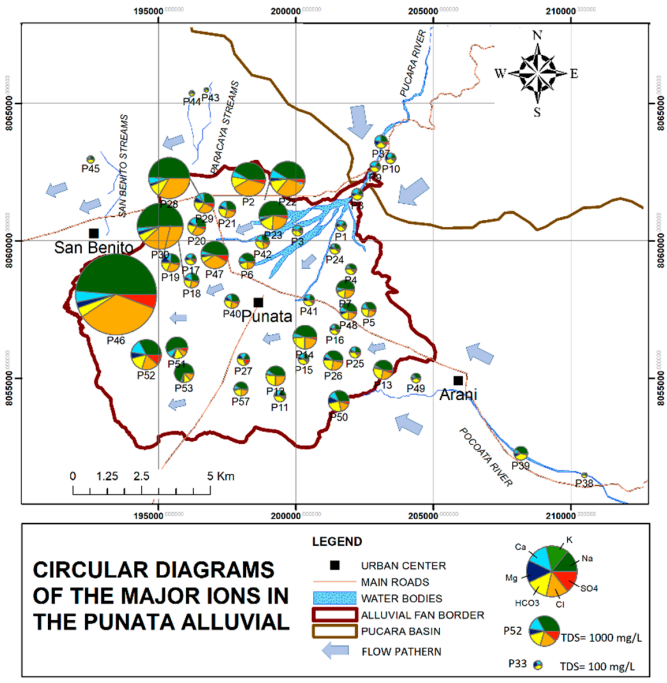

Figure 5. Circular diagrams of the water samples collected within the Punata alluvial. Note that the diameter of the circular diagrams is proportional to the total dissolved solids (TDS) content.

Another approach was used to assess hypothesis (2) and (3), which consisted in performing one-dimensional (1D) models of water infiltration in the software Hydrus-1D [44]. Daily records of precipitation from 1 August 2010 to 31 July 2017 were used to simulate the water inflow in the 1D model. Hydrus-1D besides meteorological information (e.g., precipitation) required information about soil properties. The soil samples showed that it is very likely to find a semipermeable top soil up to two meters thick composed mainly of clay and sand, with K ranging from 15 to 206 cm/day. On the other hand, pumping tests yielded K between 100 and 900 cm/day, which corresponds to layers mainly composed of coarse material [12]. Figure 6a depicts the simulation of the water content in a soil column, where it was assumed that there is a semipermeable top layer with a K of 60 cm/days (average of K values from the soil samples), the thickness of this top layer is 2 m. The rest of the column is assumed to have a K value of 500 cm/day (average K from the research of UNDP-GEOBOL [12]). Figure 6b has the same soil column characteristic as in Figure 6a, with the addition of a semipermeable layer at a depth of 10 m. This additional layer has the same properties as the top layer.

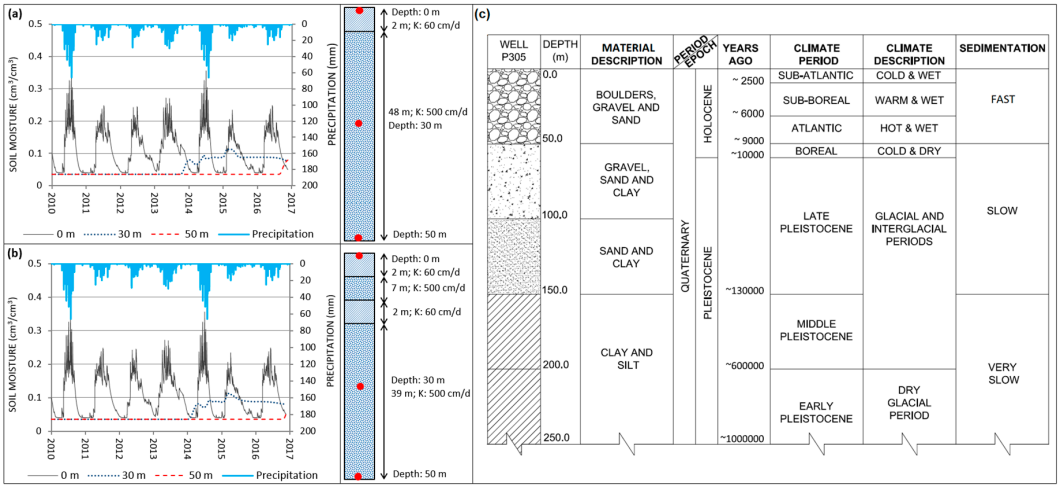

Figure 6. (**a**) Variation with time of soil water content at three different depths (i.e., 0, 30 and 50 m), and where a semipermeable layer is located at the top; (**b**) Same as in an additional semipermeable layer at depth of 10 m. Records of daily precipitation are included in each figure; (**c**) Lithological description of borehole P305 (refer to Figure 1a for location). Type of climate and rate of sedimentation are also displayed. After UNDP−GEOBOL [12].

Figure 6a,b shows that at the surface (i.e., 0 m) there are great variation in the soil moisture: after each event of precipitation, there is an increase in the soil water content, however during the dry season and due to evaporation effects the soil water content reaches the water residual content point. At a depth of 30 m, the soil water content, after four years of precipitation, barely reaches the value of 0.1, which means that the soil water content has not reached the saturation point. At the bottom of the profiles, the soil moisture remains constantly within the residual water content. The small values of the soil water content between 30 and 50 m depth highlights the assumption that water from rainfall/irrigation is not a major process within the groundwater salinization and recharge process. Therefore, it is suggested that the hypotheses (2) infiltration of irrigation waters and/or excess use of fertilizers, and (3) vertical diffuse recharge through the unsaturated soil are of minor importance in the groundwater salinization and vertical recharge. This is in line with the isotopic analysis where it is suggested that rainfall has a low role in the groundwater recharge and infiltration from rivers are the main recharge sources.

The final proposed hypothesis that could explain the high concentration of Na^+ and Cl^- ions is hypothesis (4) that suggests the existence of saline deposits, which led to a mixing of groundwater with residual pore water in the lacustrine clays and ion exchange. Figure 6c displays the lithology of

borehole P305, which is located within the head of the fan (refer to Figure 1a). The lithology description shows a decrease of grain size with depth, and a thick layer at the bottom of high clay content. In the study area, during the early Pleistocene the climate was mainly dry, therefore successive events of evaporation occurred within the former paleolakes leading to a slow sedimentation where fine particles were deposited. Also, the conditions during that period might have led to evaporated deposits or residual pore water in the bottom of the aquifer system, but when freshwater entered in contact with the evaporated deposits the first ions to be mobilized were Na^+ and Cl^-. Therefore, both ion exchange and the mixing of residual pore water in the lacustrine layers with fresh groundwater might explain the high concentration of Na^+ and Cl^-.

In order to confirm and assist in the interpretation of hypothesis (4), several geophysical campaigns were performed. The methods used were Electrical Resistivity Tomography (ERT) and Transient Electromagnetics (TEM), for more details about the surveys layout and results refer to Gonzales Amaya, Dahlin, Barmen, and Rosberg [15] and Gonzales Amaya, et al. [45]. Figure 7 shows the electrical resistivity distribution and the corresponding hydrogeological interpretation from two different areas in the Punata fan: area 1 (A-1) and area 2 (A-2), refer to Figure 1a for location. A-1 is located in the eastern part of the fan within the head and middle part of the fan, while A-2 is located in the northwestern part of the fan within the middle and distal part of the fan. The interpretation of the geophysical results showed a thick layer of coarse material within the head and middle part of the fan, while towards the distal part of the fan, the materials are predominately finer. Within the higher resistivity top layers, it is possible to observe areas of lower resistivity, which are probably thin lenses of sand and clay. As explained before, these layers might act as semipermeable or impermeable barriers preventing the vertical water infiltration (i.e., vertical transport of solutes). Moreover, both areas highlighted a very low resistivity layer close to the bottom of the aquifer system. The low resistivity values (as low as 1 Ωm in A-1, and 0.1 Ωm in A-2) might be explained by saline water stored within the finer sediments and also by the residual pore water within the lacustrine clay. Hence, the location of this saline layer indicates that hypothesis (4) can explain the origin of saline groundwater reported in some wells within the Punata alluvial fan.

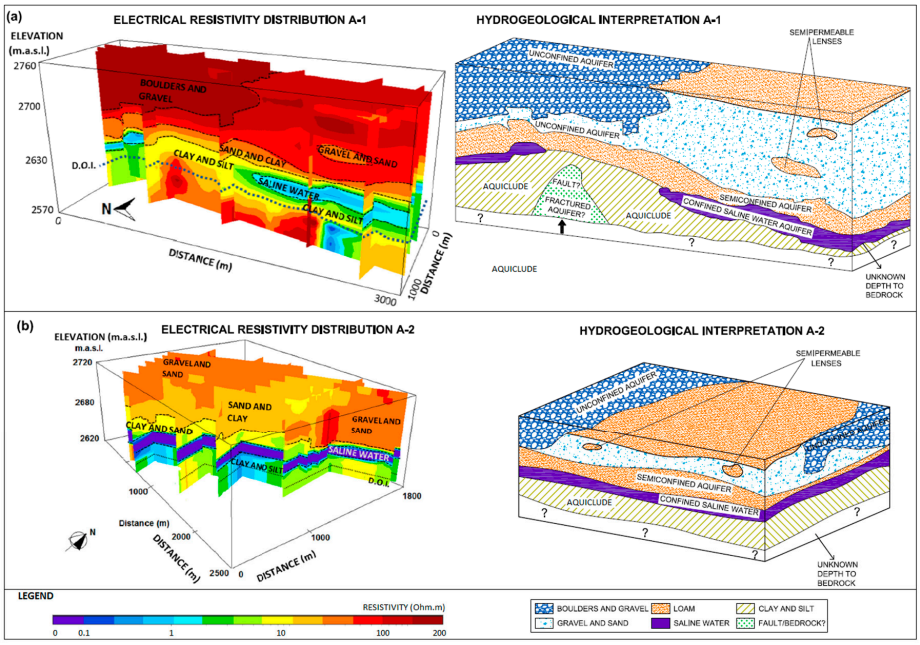

Figure 7. (**a**,**b**) Electrical resistivity and hydrogeological interpretation for A-1 and A-2, respectively (refer to Figure 1a for location).

For summarizing all of the findings of this research, a hydrogeological conceptual model is displayed in Figure 8. The hydrochemical and isotopic composition of surface waters is similar to those groundwater samples that were found in the discharge areas of Pucara and Pocoata River, highlighting the hypothesis that river flow is the main recharge source. Moreover, samples of Paracaya and San Benito streams have different isotopic signature (i.e., more depleted) and ion composition (i.e., lower TDS) than groundwater samples, suggesting that these streams do not contribute to the Punata groundwater recharge. The high concentrations of Na^+ and Cl^- of some samples indicate a salinization process within the aquifer system. At the aquifer system, bottom geophysical surveys highlighted a saline zone and a layer with high clay content. Therefore, this saline zone and high clay content layer explains the occurrence of ion exchange and that residual saline pore water are the main origins of groundwater salinization. Due to the semiarid conditions of the Punata region, evapotranspiration might had led to the deposition of solutes that could have been transported during vertical water infiltration. However, the possible location of impermeable or semipermeable lenses formed of clay and sandy clay hindered the infiltration of solutes into the groundwater. Finally, the different depths of boreholes in the northwestern part of the fan (e.g., P30 and P19 in Figure 8) can assist in explaining the higher values of TDS in some wells. For instance, P19 is deeper than P30, but the latter has higher TDS, which might be due to the fact that the P30 is closer to the aquifer bottom where the salinization activity is higher. On the other hand, P5, which is located closer to the recharge area of Pocoata River, has a lower value of TDS, and might be due to the fact that there is a thicker cap layer above the saturated zone and the bottom of the borehole is not close to the saline layer.

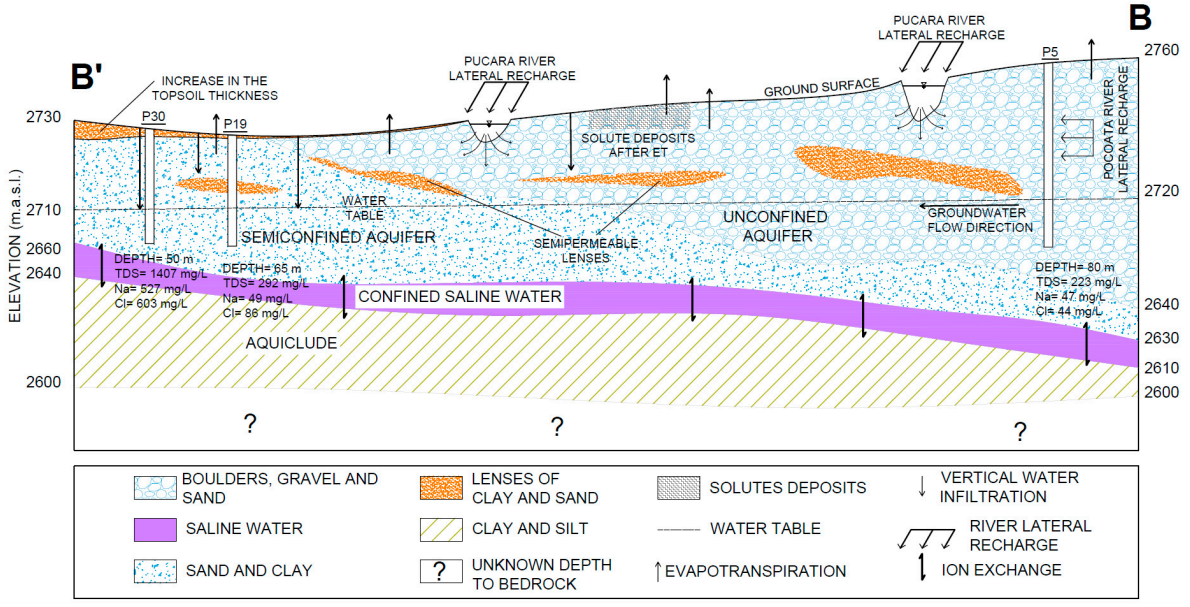

Figure 8. Hydrogeological conceptual model of the groundwater recharge and salinization processes along the section B-B′ (refer to Figure 1a for location and position of wells).

5. Conclusions

This study used the integration of the hydrochemistry of major elements, analysis of stable isotopes, modeling of 1D soil water movement, and geophysical surveys for providing a more comprehensive understanding of the recharge process and saline evolution in the Punata alluvial fan aquifer. Concentrations of Na^+ and Cl^- suggest an increase of salinization towards the distal part of the fan. Both saline residual pore water in the lacustrine sediments and ion exchange might cause groundwater to become richer with respect to Na^+ and Cl^-, rather than halite dissolution and transport of solutes from the unsaturated zone. The composition of $\delta^{18}O$ and $\delta^{2}H$ in groundwater samples are less enriched than those from precipitation. This suggests that groundwater in the Punata

fan is recharged mainly by heavy flash floods. The vertical infiltration is of less importance during the recharge process, which is probably due to semipermeable lenses within the unsaturated zone. The hydrochemical analysis also suggests that the Pucara and Pocoata rivers recharge the Punata aquifer, while the northern streams do not recharge the aquifer.

The multidisciplinary approach used in this research showed good results, because when ambiguities occurred during the interpretation process the use of other approaches helped in the final interpretation. Therefore, this study highlighted the importance of using several methods for improving the interpretation when the existing data is limited. The results that were obtained in this study will contribute in the making of policies for sustainable groundwater management in the Punata alluvial fan. However, in order to improve the knowledge of the recharge process and to verify the presented conclusions, it is recommended to take samples of the heavy flash floods and rainfall that produced these floods, and conduct an analysis of $\delta^{18}O$ and $\delta^{2}H$ composition, which includes monthly weighted rainfall and river flow. Also, it is important to conduct a comprehensive study of the mineralogy of rocks and soils within the aquifer system and nearby basin to confirm the weathering processes and mineralization processes.

Author Contributions: A.G.A. conceived the research and collected the data; A.G.A., G.B. and G.M. analyzed and wrote the paper.

Funding: This research was funded by the Swedish International Development Cooperation Agency (SIDA) under the bilateral program with Universidad Mayor de San Simon (UMSS).

Acknowledgments: The present study was supported by the Swedish International Development Agency (SIDA) and Society of Exploration Geophysicist-Geoscientists without Borders (SEG-GWB), in collaboration with Lund University (Sweden), and Universidad Mayor de San Simon (Bolivia). We are so grateful for all the support received. Special thanks to CASA-UMSS and the Geological Survey of Denmark and Greenland for taking care about the laboratory analysis of water samples.

Conflicts of Interest: The authors declare no conflict of interest.

References

1. Hassen, I.; Hamzaoui-Azaza, F.; Bouhlila, R. Application of multivariate statistical analysis and hydrochemical and isotopic investigations for evaluation of groundwater quality and its suitability for drinking and agriculture purposes: Case of Oum Ali-Thelepte aquifer, central Tunisia. *Environ. Monit. Assess.* **2016**, *188*, 1–20. [CrossRef] [PubMed]
2. Menció, A.; Mas-Pla, J.; Korbel, K.; Hose, G.C. Hydrochemical Processes in the Alluvial Aquifer of the Gwydir River (Northern New South Wales, Australia). *Procedia Earth Planet. Sci.* **2013**, *7*, 570–573. [CrossRef]
3. Zhang, B.; Song, X.; Zhang, Y.; Han, D.; Tang, C.; Yu, Y.; Ma, Y. Hydrochemical characteristics and water quality assessment of surface water and groundwater in Songnen Plain, Northeast China. *Water Res.* **2012**, *46*, 2737–2748. [CrossRef] [PubMed]
4. Burbery, L.; Vincent, C. *Hydrochemistry of South Canterbury Tertiary Aquifers*; Environment Canterbury: Christchurch, New Zeland, 2009.
5. Edmunds, W.; Droubi, A. Groundwater salinity and environmental change. In *Isotope Techniques in the Study of Environmental Change*; International Atomic Energy Agency: Vienna, Austria, 1998.
6. Fetter, C.W. *Applied Hydrogeology*, 4th ed.; Pearson: Upper Saddle River, NJ, USA, 2001; p. 598.
7. Han, D.; Liang, X.; Jin, M.; Currell, M.J.; Han, Y.; Song, X. Hydrogeochemical Indicators of Groundwater Flow Systems in the Yangwu River Alluvial Fan, Xinzhou basin, Shanxi, China. *Environ. Manag.* **2009**, *44*, 243–255. [CrossRef] [PubMed]
8. Herczeg, A.; Dogramaci, S.; Leaney, F. Origin of dissolved salts in a large, semi-arid groundwater system: Murray Basin, Australia. *Mar. Freshw. Res.* **2001**, *52*, 41–52. [CrossRef]
9. Stimson, J.; Frape, S.; Drimmie, R.; Rudolph, D. Isotopic and geochemical evidence of regional-scale anisotropy and interconnectivity of an alluvial fan system, Cochabamba Valley, Bolivia. *Appl. Geochem.* **2001**, *16*, 1097–1114. [CrossRef]

10. Yuan, R.; Song, X.; Zhang, Y.; Han, D.; Wang, S.; Tang, C. Using major ions and stable isotopes to characterize recharge regime of a fault-influenced aquifer in Beiyishui River Watershed, North China Plain. *J. Hydrol.* **2011**, *405*, 512–521. [CrossRef]
11. Kolsi, S.H.; Bouri, S.; Hachicha, W.; Dhia, H.B. Implementation and evaluation of multivariate analysis for groundwater hydrochemistry assessment in arid environments: A case study of Hajeb Elyoun-Jelma, Central Tunisia. *Environ. Earth Sci.* **2013**, *70*, 2215–2224. [CrossRef]
12. UNDP-GEOBOL. *Proyecto Integrado de Recursos Hidricos Cochabamba (Integrated Water Resources Project Cochabamba)*; United Nations Development Programme: Cochabamba, Bolivia, 1978.
13. Hernandez, C. Recarga del Abanico Aluvial de Punata (Recharge Process in the Punata Alluvial Fan). Master Thesis, Universidad Mayor Real y Pontificia de San Francisco Xavier de Chuquisaca, Sucre, Bolivia, 2012.
14. Alvarado, J.R.; Camacho, A.A.; Diaz, J.Z. *Estudy for the Control and Protection of Groundwater in Valle Alto (Cpas, bo 014901/01): Technical Report*; SERGEOMIN-TNO: Delft, The Netherlands, 1998; p. 260.
15. Gonzales Amaya, A.; Dahlin, T.; Barmen, G.; Rosberg, J.-E. Electrical resistivity tomography and induced polarization for mapping the subsurface of alluvial fans: A case study in Punata (Bolivia). *Geosciences* **2016**, *6*, 51. [CrossRef]
16. GEOBOL. *Estudio Geologico de la Hoja de Punata Cuadrangulo No. 6441 (Geological Study of Punata Region, Quadrangle No. 6441)*; GEOBOL: La Paz, Bolivia, 1983.
17. May, J.-H.; Zech, J.; Zech, R.; Preusser, F.; Argollo, J.; Kubik, P.W.; Veit, H. Reconstruction of a complex late quaternary glacial landscape in the Cordillera de Cochabamba (Bolivia) based on a morphostratigraphic and multiple dating approach. *Quat. Res.* **2011**, *76*, 106–118. [CrossRef]
18. American Public Health Association (APHA). *Standard Methods for the Examination of Water and Wastewater*; American Public Health Association-America Water Works Association-Water Environment Federation: Washington, DC, USA, 1995.
19. Parkhurst, D.L.; Appelo, C. *User's Guide to Phreeqc (Version 2): A Computer Program for Speciation, Batch-Reaction, One-Dimensional Transport, and Inverse Geochemical Calculations*; Water-Resources Investigations Report; U.S. Geological Survey: Reston, VA, USA, 1999.
20. Reynolds, W.; Elrick, D. A laboratory and numerical assessment of the Guelph permeameter method. *Soil Sci.* **1987**, *144*, 282–299. [CrossRef]
21. Elrick, D.; Reynolds, W.; Tan, K. Hydraulic conductivity measurements in the unsaturated zone using improved well analyses. *Groundw. Monit. Remediat.* **1989**, *9*, 184–193. [CrossRef]
22. Schaap, M.G.; Leij, F.J.; Van Genuchten, M.T. Rosetta: A computer program for estimating soil hydraulic parameters with hierarchical pedotransfer functions. *J. Hydrol.* **2001**, *251*, 163–176. [CrossRef]
23. Chadha, D. A proposed new diagram for geochemical classification of natural waters and interpretation of chemical data. *Hydrogeol. J.* **1999**, *7*, 431–439. [CrossRef]
24. Han, D.; Kohfahl, C.; Song, X.; Xiao, G.; Yang, J. Geochemical and isotopic evidence for palaeo−seawater intrusion into the south coast aquifer of Laizhou Bay, China. *Appl. Geochem.* **2011**, *26*, 863–883. [CrossRef]
25. Edmunds, W.; Ma, J.; Aeschbach-Hertig, W.; Kipfer, R.; Darbyshire, D. Groundwater recharge history and hydrogeochemical evolution in the Minqin Basin, North West China. *Appl. Geochem.* **2006**, *21*, 2148–2170. [CrossRef]
26. Herczeg, A.; Torgersen, T.; Chivas, A.; Habermehl, M. Geochemistry of ground waters from the Great Artesian Basin, Australia. *J. Hydrol.* **1991**, *126*, 225–245. [CrossRef]
27. Appelo, C.A.J.; Postma, D. *Geochemistry, Groundwater and Pollution*; CRC Press: Boca Raton, FL, USA, 2004.
28. Marion, G. The geochemistry of natural waters: Surface and groundwater environments. *J. Environ. Qual.* **1998**, *27*, 245. [CrossRef]
29. Drever, J.I. *The Geochemistry of Natural Waters*; Prentice Hall: Englewood Cliffs, NJ, USA, 1988.
30. Datta, P.; Tyagi, S. Major ion chemistry of groundwater in Delhi area: Chemical weathering processes and groundwater flow regime. *J. Geol. Soc. India* **1996**, *47*, 179–188.
31. Bouzourra, H.; Bouhlila, R.; Elango, L.; Slama, F.; Ouslati, N. Characterization of mechanisms and processes of groundwater salinization in irrigated coastal area using statistics, GIS, and hydrogeochemical investigations. *Environ. Sci. Pollut. Res.* **2015**, *22*, 2643–2660. [CrossRef] [PubMed]
32. García, G.; Hidalgo, M.; Blesa, M. Geochemistry of groundwater in the alluvial plain of Tucuman province, Argentina. *Hydrogeol. J.* **2001**, *9*, 597–610. [CrossRef]

33. Jalali, M. Major ion chemistry of groundwaters in the Bahar area, Hamadan, western Iran. *Environ. Geol.* **2005**, *47*, 763–772. [CrossRef]
34. Kendall, C.; Caldwell, E.A. Fundamentals of isotope geochemistry. In *Isotope Tracers in Catchment Hydrology*; Kendall, C., McDonnell, J.J., Eds.; Elsevier Science: Amsterdam, The Netherlands, 1998; pp. 51–86.
35. Craig, H. Isotopic variations in meteoric waters. *Science* **1961**, *133*, 1702–1703. [CrossRef] [PubMed]
36. Mook, W.; Rozanski, K. *Environmental Isotopes in the Hydrological Cycle*; International Atomic Energy Agency: Vienna, Austria, 2000; p. 39.
37. IAEA. *Atlas of Isotope Hydrology—The Americas*; International Atomic Energy Agency: Vienna, Austria, 2009.
38. Solis, G.; Araguas, L. Study of groundwater in the Cochabamba Valley (Bolivia) using isotope techniques. In *Isotope Hydrology Investigations in Latin America 1994*; International Atomic Energy Agency: Vienna, Austria, 1995.
39. Gonfiantini, R.; Roche, M.-A.; Olivry, J.-C.; Fontes, J.-C.; Zuppi, G.M. The altitude effect on the isotopic composition of tropical rains. *Chem. Geol.* **2001**, *181*, 147–167. [CrossRef]
40. Aravena, R.; Peña, H.; Grilli, A.; Suzuki, O.; Mordeckai, M. Evolución isotópica de las lluvias y origen de las masas de aire en el altiplano chileno (isotopic evolution of rainfall and the origin of air masses in the chilean altiplano). In *Isotope Hydrology Investigations in Latin America*; International Atomic Erengy Agency: Vienna, Austria, 1989; pp. 129–142.
41. Rozanski, K.; Araguás-Araguás, L.; Gonfiantini, R. Isotopic patterns in modern global precipitation. In *Climate Change in Continental Isotopic Records*; American Geophysical Union: Washington, DC, USA, 1993; pp. 1–36.
42. Lizarazu, J.; Aranyossy, J.; Orsag, V.; Salazar, J. Estudio isotópico de la cuenca de Oruro-caracollo, bolivia (isotopic study in the Oruro-Caracollo watershed, Bolivia). In *Isotope Techniques in Water Resources Development, Proceeding of Symposium, Vienna, Austria, 30 March–3 April 1987*; International Atomic Energy Agency: Vienna, Austria, 1987; pp. 301–304.
43. Gat, J.R. Oxygen and hydrogen isotopes in the hydrologic cycle. *Annu. Rev. Earth Planet. Sci.* **1996**, *24*, 225–262. [CrossRef]
44. Simunek, J.; Van Genuchten, M.T.; Sejna, M. *The Hydrus-1d Software Package for Simulating the One-Dimensional Movement of Water, Heat, and Multiple Solutes in Variably-Saturated Media*; University of California−Riverside Research Reports: Oakland, CA, USA, 2005; Volume 3, pp. 1–240.
45. Gonzales Amaya, A.; Mårdh, J.; Dahlin, T. Delimiting a saline water zone in Quaternary fluvial–alluvial deposits using transient electromagnetic: A case study in Punata, Bolivia. *Environ. Earth Sci.* **2018**, *77*, 46. [CrossRef]